Endothelial Cell Adhesion in Real Time

Measurements In Vitro by Tandem Scanning Confocal Image Analysis

Peter F. Davies,* Andre Robotewskyj,* and Melvin L. Griem‡
*Departments of *Pathology and ‡Radiation and Cellular Oncology, Pritzker School of Medicine, The University of Chicago, Chicago, Illinois 60637*

Abstract

Real time measurements of cell-substratum adhesion in endothelial cells were obtained by tandem scanning confocal microscopy of sites of focal contact (focal adhesions) at the abluminal cell surface. Focal contact sites were sharply defined (low radiance levels) in the living cell such that the images could be enhanced, digitized, and isolated from other cellular detail. Sites of focal contact are the principal determinant of cell-substratum adhesion. Measurements of (*a*) the focal contact area and (*b*) the closeness of contact (inverse radiance) were used to nominally define the adhesion of a single cell or field of cells, and to record spontaneous and induced changes of cell adhesion in real time.

The topography of focal contacts was estimated by calculating separation distances from radiance values using a calibration technique based on interference ring optics. While slightly closer contact was noted between the cell membrane and substratum at or near the center of each focal contact, separation distances throughout the adhesion regions were always < 50 nm.

Subtraction of consecutive images revealed continuous spontaneous remodeling of individual focal adhesions in unperturbed cells during periods of < 1 min. Despite extensive remodeling of focal contact sites, however, cell adhesion calculated for an entire cell over extended periods varied by < 10%. When cytoskeletal stability was impaired by exposure to cytochalasin or when cells were exposed to proteolytic enzyme, endothelial adhesion declined rapidly. Such changes were recorded at the level of single cells, groups of cells, and at single focal adhesions. In both unperturbed and manipulated cells, the dynamics of remodeling and cell adhesion characteristics varied greatly between individual sites within the same cell; disappearance of existing sites and appearance of new ones often occurred within minutes while adjacent sites underwent minimal remodelling.

Tandem scanning confocal microscopy image analysis of living cells in real time provides repetitive spatial, temporal, and quantitative information about cell adhesion. Such an approach should allow more precise quantitative analyses to be made of the interactions between extracellular matrix, adhesion proteins, integrins, and the cytoskeleton in the living cell. (*J. Clin. Invest.* 1993. 91:2640–2652.) Key words: focal contacts • focal adhesions • adhesion dynamics

Introduction

Regions of focal contacts and close contacts between the abluminal cell surface and the extracellular substratum are the sites primarily responsible for cell adhesion. They are involved in the regulation of cell morphology, proliferation, migration, differentiation, and responsiveness (1), and provide anchorage sites essential for the maintenance of tension within the cell (2). Focal contact sites are associated with the insertion of actin stress fibers on the cytoplasmic side of the plasma membrane and an array of intracellular linker proteins, transmembrane integrins, and extracellular adhesion proteins that connect the cytoskeleton to the extracellular matrix (3–5). Paddock (6) has recently described the use of tandem scanning confocal microscopy (TSCM)[1] to observe focal contacts in Swiss 3T3 cells when the microscope is operated in the reflected light mode. In this application, the TSCM operates on similar principles to interference reflection microscopy (IRM) such that light is reflected from the aqueous layer lying between the cell membrane and the substratum when the two materials are apart, but when the two are in close apposition, reflected radiance levels sharply decline and the focal contacts appear dark grey to black. A substantial advantage of TSCM over IRM is the optical sectioning capability afforded by confocal microscopy. By positioning the optical plane to include only the abluminal cell surface, other cellular detail is excluded. Both TSCM and IRM provide real time images of adhesion sites in living cells. The recent availability of image enhancers, sensitive charge-coupled devices video cameras, and sophisticated computer-based image processing and analysis capabilities, permits the collection of digitized image information for qualitative and quantitative analysis.

In 1966, Stehbens (7) noted electron dense regions near the plasma membrane of frog endothelial cells which resisted detachment during cell injury. Subsequently, Abercrombie et al. (8) in fibroblasts and Ts'ao and Glagov (9) in rabbit artery endothelium observed microfilaments associated with these regions that anchor the cell to the abluminal extracellular connective tissue. Endothelial cells are particularly suitable for studies of cell adhesion because they define the blood vessel/plasma boundary and are polarized cells that attach to the sub-

A preliminary report of parts of this work has appeared in abstract form (1991. *FASEB (Fed. Am. Soc. Exp. Biol.) J.* 5:1603A).

Address correspondence to Peter F. Davies, Ph.D., The University of Chicago, Department of Pathology, MC6079, 5841 South Maryland Avenue, Chicago, IL 60637.

Received for publication 14 September 1992 and in revised form 19 January 1993.

J. Clin. Invest.

0021-9738/93/06/2640/13 $2.00
Volume 91, June 1993, 2640–2652

1. *Abbreviations used in this paper:* BAEC, bovine aortic endothelial cells; F-actin, filamentous actin; HUVE, human umbilical vein endothelial cells; IRM, interference reflection microscopy; TSCM, tandem scanning confocal microscopy.

stratum on the abluminal side only. Their biology is markedly influenced by cell shape which in turn is largely determined by membrane interactions with the substratum (10–13). Endothelial adhesion properties are also important in efforts to create successful prosthetic vascular grafts (14) and in the regeneration of endothelial coverage following surgical trauma. Although the isolation of focal adhesions and purification of their components has provided much structural and biochemical information (15), dynamic information about endothelial cell adhesion is very limited, as is detailed information about the relationships between focal adhesion sites, cell morphology, and cell function in living cells. Qualitative estimates of the distribution of adhesion sites have been made by immunofluorescence localization of adhesion-specific proteins (reviewed in reference 1) and by IRM (3, 16–18), but the study of individual components in the kinetics of adhesion is limited by the sensitivity of quantitative assays. Cell adhesion is usually measured as the number of cells that attach and flatten, or the cells remaining attached after exposure to physical forces such as flow (14) or centrifugation (19). These are one-time assays that do not repeatedly measure the same cells.

In this paper, TSCM images of focal contact sites were obtained and then enhanced, digitized, and processed by image analysis procedures to provide spatial, temporal, and quantitative information about focal contacts and cell adhesion in endothelial cells in real time. Spontaneous rapid remodeling of these sites was observed and measured, the topography of adhesion regions was estimated, a method for consecutive measurements of adhesion in living cells was developed, and the dynamics of focal contact sites during the disruption of adhesion by recognized manipulations was examined.

Methods

Cell culture

Bovine aortic (BAEC) or human umbilical vein endothelial cells (HUVE) were isolated and grown to passage 7–20 (BAEC) or 1–3 (HUVE) using standard procedures (20, 21). After trypsinization, the cell suspension was plated at subconfluent density into 1 mm × 1 mm square cross-section borosilicate glass capillary flow tubes (22) (Vitro Dynamics, Rockaway, NJ) which either were untreated (BAEC) or precoated with 0.1% gelatin (HUVE). The thickness of the gelatin layer, a contributor to the cell–glass separation distance, was measured as 6 nm±1 nm by atomic force microscopy (Barbee, K., R. Lal, and P. F. Davies; unpublished). BAEC were bathed in DME (high glucose; Gibco Laboratories, Grand Island, NY) containing 10 mM Hepes, 2 mmol/ml glutamine, 100 U/ml penicillin, 100 μg/ml streptomycin, and 10% heat inactivated calf serum (Gibco Laboratories). After the cells had plated on one wall of the tube, all subsequent routine medium changes were conducted by capillary exchange. In some studies, cells were grown on glass cover slips (Bellco Biotechnology, Vineland, NJ) using standard procedures. Glass surfaces were not further pretreated other than by serum-containing medium at the time of plating. Subconfluent cells were typically used 1 d after plating and confluent cells after 1 wk in culture.

Confocal microscopy

Phase contrast and confocal images were viewed using a tandem scanning confocal microscope (Noran Instruments, Inc., Middleton, WI) equipped with long working distance Zeiss Planapo ×40 and Neofluar ×100 oil immersion lenses with high numerical apertures (1.0 and 1.25, respectively) to concentrate the available light and to provide images constituted from zero-order interferences (see below). Cells were observed from outside of the capillary tube. To maintain pH and facilitate nutrient supply and waste removal in the tubes, three tube-volume changes per minute were maintained by slow perfusion (150 μl/min) using a closed flow circuit driven by a peristaltic pump (Harvard Apparatus, S. Natick, MA) with appropriate pulse dampening, pH, and temperature control systems. The optical plane of the TSCM (0.7-μm thickness) was positioned just below the cell and raised until it overlapped the interface between the cell and substratum. Images from the TSCM were directed via an intensified charged-couple devices video camera (Videoscope International, Washington, DC) and relay lens to produce an analogue video signal that was digitized and converted to 640 × 480 pixels by an image analysis system (QX-7 214; Quantex Corp., Sunnyvale, CA). Images were collected in real time, averaged to reduce noise and increase sharpness, and corrected for uneven illumination. Image analyses of adhesion sites were conducted by radiance analysis procedures that measured the area of each adhesion site, its radiance and location, using Quantex image recording and analysis software routines. To calculate adhesion from area and radiance measurements, additional subroutines were written. Focal contacts were identified by the large decrease in radiance level associated with them; this allowed elimination of other image detail by gray level thresholding. The resolution of detection of focal contacts was dependent upon the resolution of the computer screen (3.07×10^5 pixels^2) and the magnifying power of the objective lens (usually ×100). With this arrangement, a single pixel represented 2×10^{-2} μm^2. Further processing of images was conducted on a Macintosh IIfx computer (Apple Computer, Copertino, CA).

Spatial estimates between the cell and substratum at adhesion sites (topography of adhesion)

Bead model. A polystyrene bead was pressed against a glass surface and observed by TSCM; interference fringes occurred at radial intervals around the contact site (Fig. 1 *A*). The fringes were generated by alternate constructive and destructive interference of out-of-phase light paths as the separation distances between bead and glass increased. The refractive indices of the bead, culture medium, and the glass were 1.59, 1.33, and 1.53, respectively. The radiance minima occurred at separation distance periods of one-half wavelength ($\lambda/2$; in this case $^{650}/2$ nm) where destructive interference occurred. Thus the first dark ring outside of the area of contact occurred when the distance between bead and glass was 325 nm. Between the dark rings were radiance maxima (constructive interference) also with a periodic separation distance of $\lambda/2$; thus the radiance differences between minima and maxima occurred with $\lambda/4$ (163 nm) periodicity. Radiance values were plotted as a function of separation distance between the region of contact (zero order minimum, 0 nm separation distance) to the first order maximum fringe at $\lambda/4$ (163 nm) as shown in Fig. 1 *a–c*.

Cell model. To observe greater than first order interference minima fringes in a cell, the separation distance between the abluminal cell membrane and the glass must exceed $\lambda/2$ (325 nm). This is uncommon underneath the body of the cell except where a process may become partially detached or a ruffling membrane separates near a leading edge. Occasionally, however, we were able to locate a first order fringe, an example of which is shown in Fig. 1 *B*. A plot of radiance value between the zero order minimum and first order maximum in this cell revealed a similar plot to that observed in the bead model except that the zero order minimum was set at 15 nm instead of zero (Fig. 1, *d–f*). This decision was based upon electron micrographs that indicate the separation distances within focal adhesions of fixed cells to be of the order of 15–30 nm. The calibration curve obtained from the living cell was linearized by transformation and stored in computer memory for referencing radiance/separation distances within the same cell as well as in other cells in the same field. A program was written to automatically calculate the separation distance when a cursor was positioned over different parts of the cell. Thus an estimate of the spatial relationship between cell and substratum was obtained.

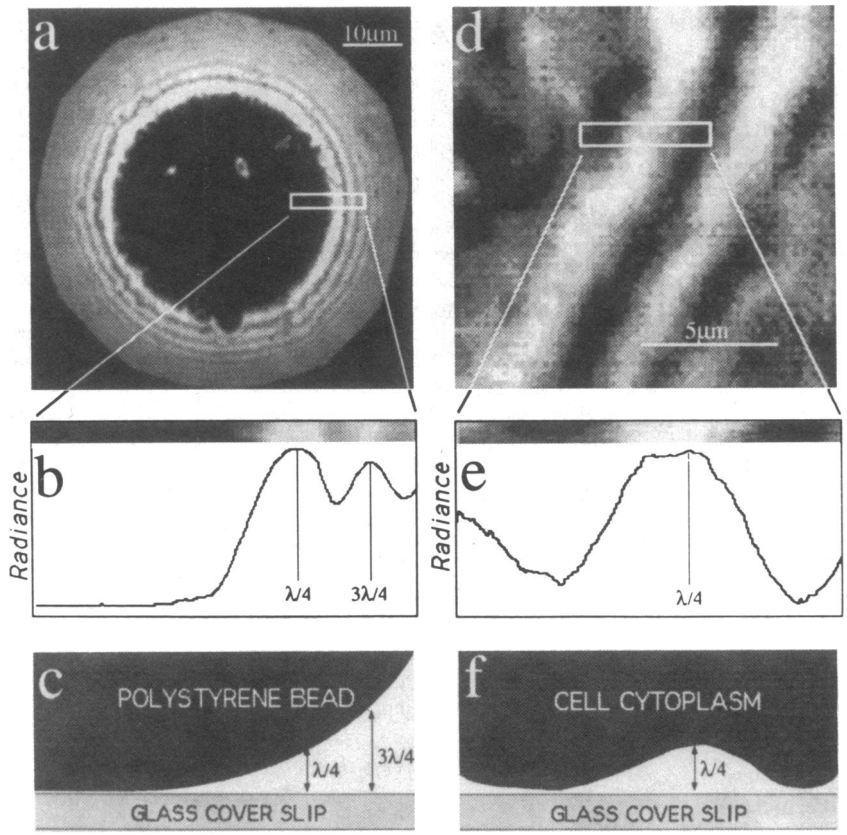

Figure 1. Interference fringes in (*a–c*) a polystyrene bead pressed into contact with a glass substratum, and (*d–f*) within an endothelial cell. The radiance plots obtained from within the cell were used to calibrate separation distances between the cell and the glass substratum as outlined in Methods.

Fluorescence staining

Cells were fixed with 4% formaldehyde in PBS for 20 min at 37°. After three washes with PBS, the cells were permeabilized by 0.1% Triton X-100 in PBS for 3 min at room temperature, washed twice with PBS, then three times with 50 mM ammonium chloride, pH 7.3, for 5 min each wash. After rinsing twice with PBS, nonspecific binding was blocked by 0.1% BSA in PBS for 30 min, after which the cells were incubated with antivinculin or antitalin antibody (monoclonal; Sigma Chemical Co., St. Louis, MO) at a dilution of 1:50–1:500. After three washes with PBS, FITC-conjugated rabbit anti-mouse immunoglobulin (50 μg/ml) was added for 30 min at room temperature. Normal serum IgG was used as a negative control for the primary antibody. Filamentous actin (F-actin) was stained by addition of NBD-phallacidin (23) (Molecular Probes, Inc., Eugene, OR) at a dilution in PBS of 1:100 of a 3-mM stock solution, for 20 min at room temperature, followed by three final washes in PBS. Cells either on coverslips (mounted in 1:10 glycerol:PBS containing 2 mg/ml *p*-phenyldiamine) or in capillary tubes were viewed using a Leitz fluorescence microscope equipped with epifluorescence, or the TSCM using a Xenon light source and narrow band pass filters for fluorescein and rhodamine excitation-emission (Omega Optical Co., Burlington, VT).

Additional photomicrographs were obtained using an Olympus IMT-2 inverted microscope in phase contrast mode. Cell images were photographed on 35-mm Kodak T-Max film, ASA 400, or Fuji ASA 3,200 film, by directing the light path to an Olympus OM-4 camera attached to either the TSCM or the Olympus inverted microscope, or a Leitz photomicrographic system (Leitz vario orthomat; ×40/0.9 NA, ×100/1.1 NA lenses) for nonconfocal fluorescence image recording. Digitized, processed confocal images were photographed directly from the monitor screen using a Nikon F2 camera with 55-mm macro lens and 35-mm Kodak Ektachrome film ASA 100, or were routed directly to a color printer.

Electron microscopy

Cells were fixed, dehydrated, and embedded as previously described (23). Transverse sections, stained lightly with lead citrate, were examined in a Philips 201 microscope. Ruthenium red (0.05%; Sigma Chemical Co.) was included in both glutaraldehyde and osmium fixatives at 4° to enhance the plasma membrane.

Cell perturbation

Cytochalasin B (Sigma Chemical Co.) or trypsin:EDTA (Gibco Laboratories) was infused into capillary flow tubes at concentrations of 10 μg/ml and 0.1%:2 mM, respectively. The flow tube configuration permitted rapid exchange of these agents which are disruptive to focal contact morphology. Consecutive TSCM images of single cells were captured at intervals of 1 min for cytochalasin and 20 s for trypsin:EDTA. Qualitative and quantitative image analysis was performed as described above and in Results.

Results

TSCM of focal contacts in endothelial cells

When the optical plane of the TSCM was positioned at the abluminal cell surface, black regions of focal contacts and gray regions of close contacts were observed (Fig. 2). The low radiance at these sites occurs because of a zero order interference pattern such that inverse radiance levels were proportional to the closeness of contact between cell and substratum within a range of separation distances extending from 0 to 100 nm (13, 24). Cellular detail unrelated to adhesion sites was minimized because of the restricted optical plane, a distinct advantage over IRM (see Paddock for discussion of TSCM in IRM mode,

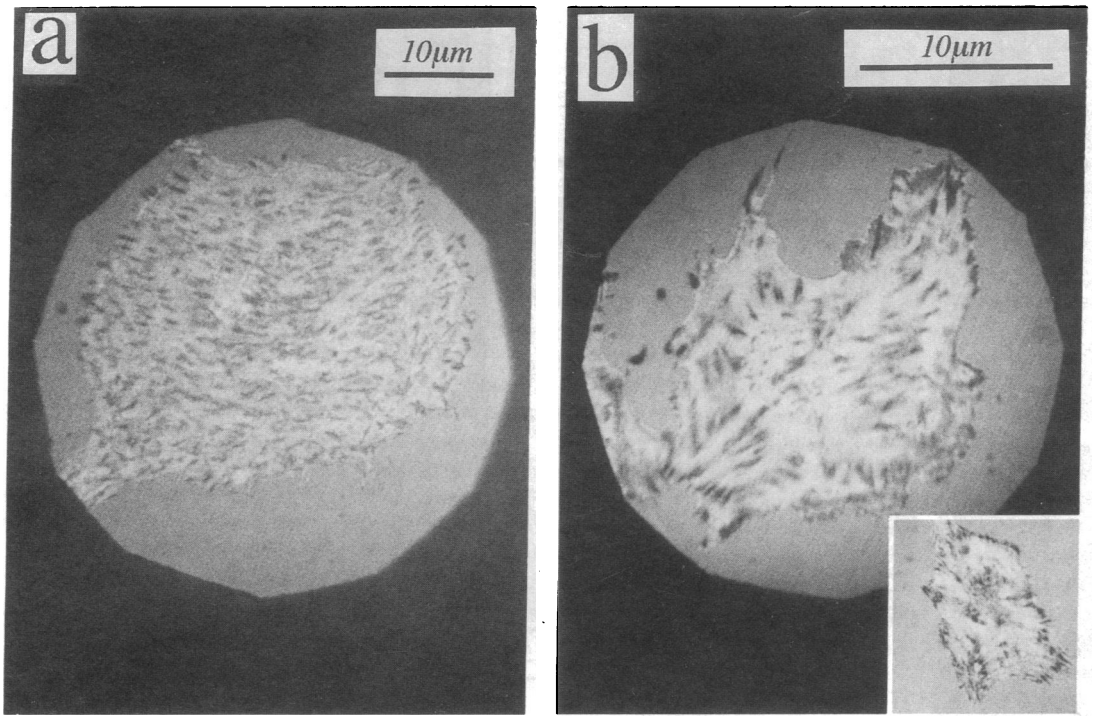

Figure 2. TSCM images of single bovine aortic endothelial cells in tissue culture. In (*a*), focal contact sites are distributed fairly uniformly throughout the cell whereas more polarized (*b*) and migrating (*inset b*) cells express heterogeneous focal contacts preferentially localized to the peripheral lamellae. Inset ×400.

and Verschueren for a critical discussion of IRM; references 6 and 24). At focal contacts, the ventral plasma membrane approaches within 10–15 nm of the glass (13), greatly increasing light transmission and decreasing reflected light levels. Close contact regions, which appeared gray, have been estimated to represent a gap of 30–100 nm (13, 24). Focal contacts were sometimes evenly distributed throughout the cell (Fig. 2 *a*); more often the distribution was uneven (Fig. 2 *b*). They varied in number and location from cell to cell, occurring preferentially at or near the leading edge of migrating cells (Fig. 2 *b, inset*). There was a heterogeneous distribution within any single cell, both with respect to size and shape. Focal adhesion sites varied in area from the smallest detectable in this system (single pixel resolution, 2×10^{-2} μm^2) to elongated sites several microns long by up to 1 μm wide, dimensions that were similar to those noted using IRM (16) and by Paddock using TSCM (6). A histogram of the size distribution of 467 focal contact regions in bovine aortic endothelial cells is shown in Fig. 3. The distribution is weighted towards smaller sized sites with the highest percentage in the smallest size range, < 2 μm^2 (< 50 square pixels), and 79% of the total were < 6 μm^2 (300 square pixels).

Focal contacts in confluent endothelial cells, which are in a nonproliferative and nonmigratory state, were generally less aligned than those in single cells (Fig. 4). When confluence was maintained for several weeks, the frequency of focal contacts in the cell declined, accompanied by increased frequency of close contacts rather than focal contacts (not shown). However, for the studies of confluent cells reported here, the cells were routinely used within 3 d of attaining confluence and demonstrated prominent focal contacts.

The percentage of the total abluminal cell surface area that was involved in adhesion (focal and close contact regions) in subconfluent and confluent cells was 21.6%±3.6 (SD; $n = 4$), and 16.2%±5.7 (SD; $n = 8$), respectively; significantly different, $P < 0.05$.

Immunofluorescence and electron microscopy

F-actin filaments frequently appeared to terminate at the abluminal surface of the cell (Fig. 5 *a*), presumably reflecting the association of cytoskeletal elements with alpha-actinin which in turn binds to β integrin (25, 26). Actin microfilaments also may associate with other cytoplasmic linker proteins (talin, vinculin, paxillin) at focal adhesion sites (1, 27). Although the

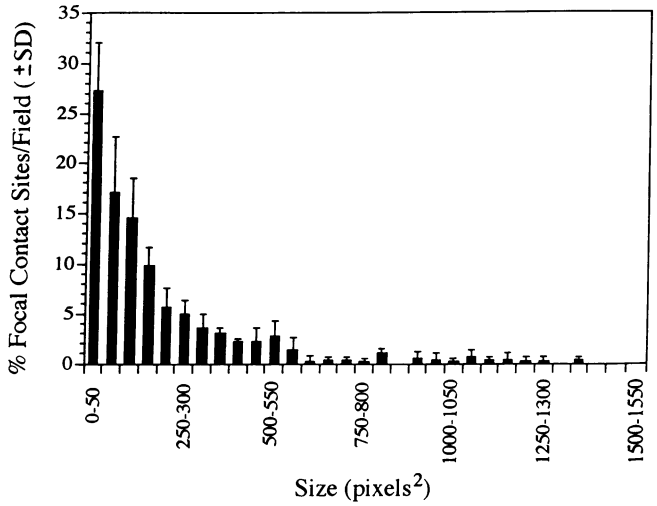

Figure 3. Distribution of sizes of focal contact regions in a field of confluent endothelial cells (one to two cells/field). Each column is the percentage (mean±SD) of all focal adhesion sites in each size range (pixel area). One pixel corresponds to 2×10^{-2} μm^2. Values derived from three experiments; $n = 467$.

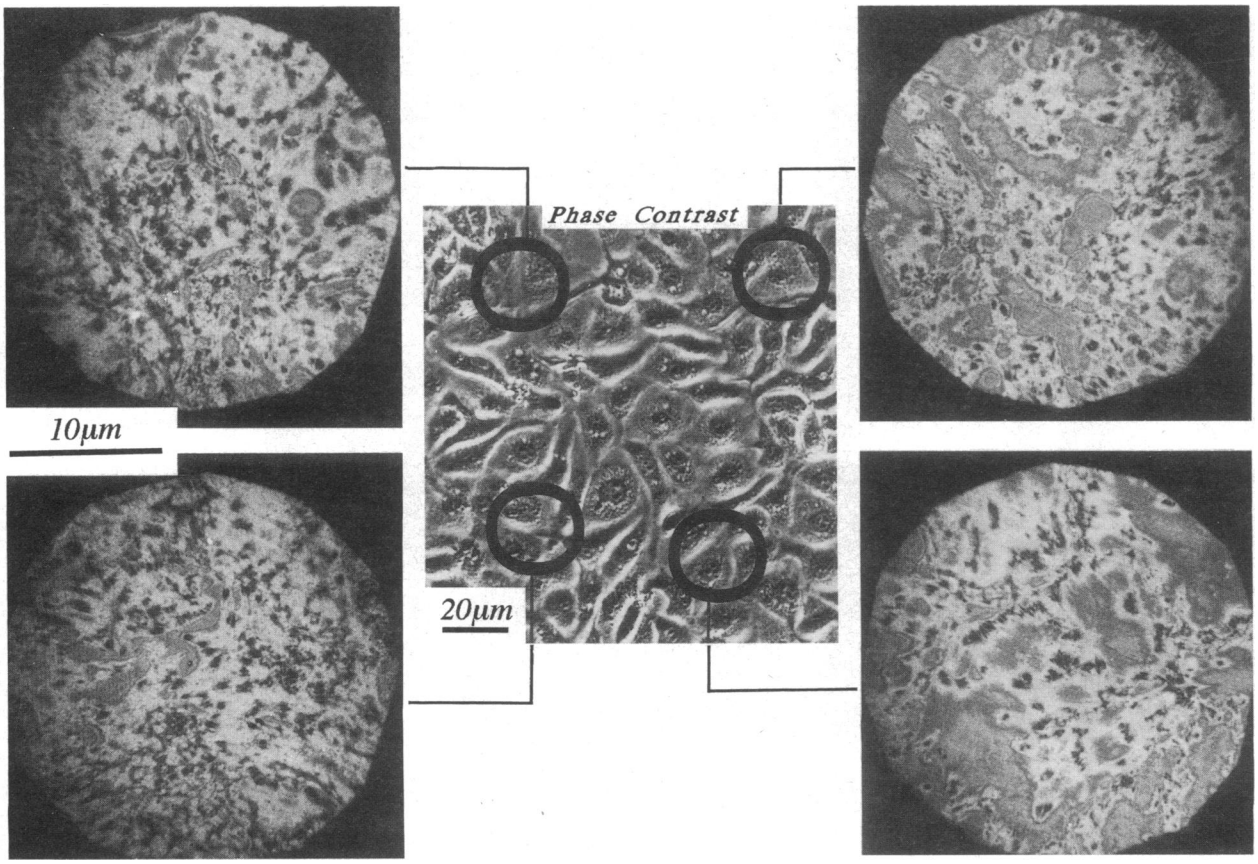

Figure 4. TSCM images of confluent endothelial cells. Four regions of the confluent monolayer are shown 5 d after confluence was attained. In addition to regions of focal contact, close contact areas (gray) are broadly distributed throughout each field. There are considerable differences in the number and intensities of adhesion sites in cells within the same monolayer. In the confocal images, each of which represents one to two cells, the cell boundaries are not visible.

sensitivity of the TSCM was insufficient for optical sectioning of F-actin fluorescence, recent studies using the latest versions of laser confocal microscopy have suggested filament termination at the regions of focal contact (Dissanayake, S., and E. Chang, personal communication), observations that are also in agreement with the conclusions of others using different approaches (3–5). The cellular distribution of vinculin (and talin) observed by immunofluorescence microscopy was similar to that of focal adhesion sites (Fig. 5 *b*). Transmission electron microscopy of transverse sections of focal contact sites also revealed increased density of microfilaments at the cytoplasmic face (Fig. 5 *c*) in agreement with published observations (1–4).

Qualitative information obtained from TSCM images

Gray level thresholding was used to define the focal adhesions whose well-resolved borders coincided with a sharp decline in radiance values. The threshold value was set for the initial cell image and maintained unchanged for the duration of each experiment. TSCM images were digitized and focal contact regions were extracted by exclusion of radiance levels above the threshold value. The residual radiance scale was then expanded by assigning a full range of values from 0 to 255 and expressed in pseudocolor to amplify the small differences in radiance within each contact region. The resulting images could be superimposed on phase contrast images of the same cell (Fig. 6, *a–c*).

Profiles of individual focal contact sites. When radiance profiles were obtained from TSCM images of focal contact sites, we noted that light levels along the profile were variable. Radiance levels were converted to a color scale (Fig. 6 *d*). It should be noted, however, that the entire pseudocolor spectrum represents an expanded narrow range of radiance values and that all of the contact region represents very close apposition of cell membrane to the substratum. Both the pseudocolor distribution (Fig. 6 *d*) and the profile plots (Fig. 6 *e*) demonstrated slightly closer contact at the interior of each site; more than one maximal contact peak was often observed within a confluent focal adhesion (an example is shown in Fig. 6 *d*). However, the difference in separation distance between cell and substratum at the edge of a focal contact site as compared with one near its center was estimated to be small (see below).

Spatial relationships between cell and substratum. The topographic mapping of a small area (14×14 μm) of abluminal cell membrane which includes several focal adhesion sites is shown in Fig. 7. Radiance levels were converted to separation distances by the interference fringe technique described in Methods. The scale of the peaks and valleys (z axis) is exaggerated in this figure compared with the scale of the area axes to amplify the topology. In the regions of focal contact, separation

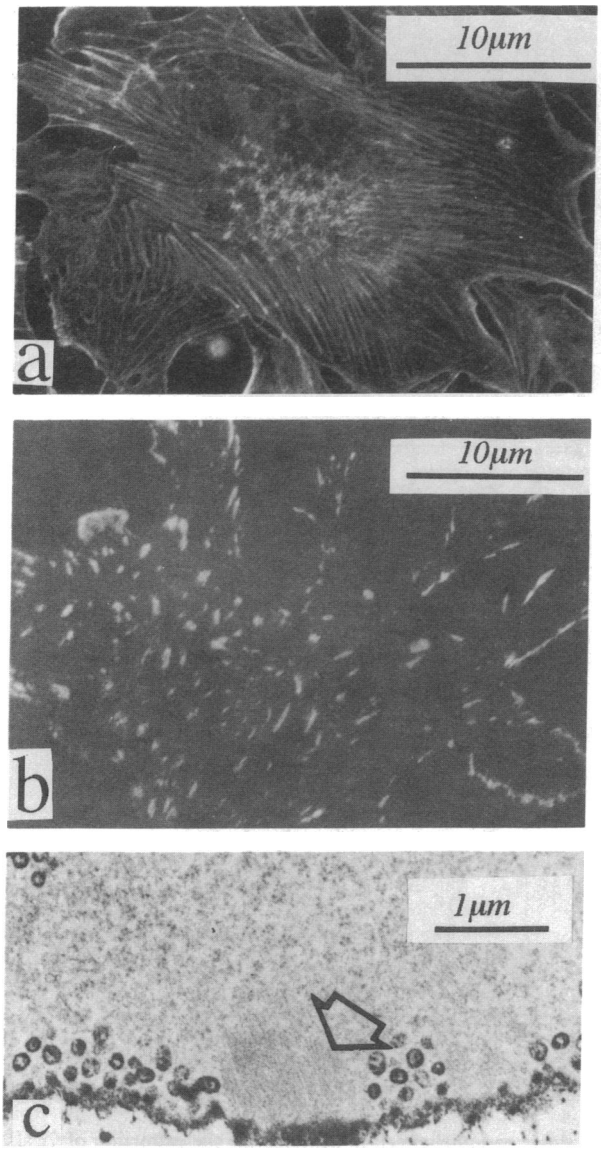

Figure 5. Subconfluent endothelial cells stained for F-actin (*a*) and vinculin (*b*). Stress fibers terminate at multiple sites throughout the cell including the ventral cell membrane (3, 4). Two different cell preparations are shown. The distribution of vinculin is similar to that of focal contact regions. (*c*) Transmission electron micrograph of the abluminal side of a bovine aortic endothelial cell attached to glass. An extensive microfilament network (*arrowhead*) is visible in the cytoplasm adjacent to and interacting with an adhesion site. Plasma membrane invaginations and vesicles are absent at these sites. A second smaller focal contact site, also rich in filamentous material, and that has separated slightly from the substratum during tissue processing is visible to the right. The plasma membrane glycocalyx was decorated with ruthenium red (after fixation) in this preparation.

distances in the range 10–50 nm were recorded, consistent with estimates from IRM and transmission electron microscopy. At the boundaries of adhesion sites there was a sharp increase of separation distance. Gradients measured from transverse profiles of individual sites averaged 5.5±2.6 nm per 0.1 μm horizontal distance (n = 8) consistent with the profiles obtained from adhesion sites observed in transmission electron micrographs. Near the center of focal contact sites where separation distances were minimal, occasional regions of multiple "point" contact were noted (Fig. 8). These images may reflect stress fiber termination sites within the focal adhesion.

Remodeling of focal contact regions in real time. Focal contact regions are dynamic structures even in quiescent, unperturbed endothelial cells. Remodeling, visualized by image subtraction, was observed within as brief a period as 15 s. Two images (*im*) separated by an interval (t_2–t_1) were collected. Subtraction of *im* 1 from *im* 2 revealed additions to existing sites, while *im* 1 minus *im* 2 showed focal contact area that had disappeared during the same period. The results of each subtraction were expressed in different colors and superimposed upon the original unprocessed image. The assembled image in Fig. 9, therefore, outlines the original location of focal contacts (blue) and the areas of addition (red) and disappearance (yellow) that occurred during the remodeling interval. Fig. 9 demonstrates remodeling during periods of 5, 10, and 30 min in an undisturbed single endothelial cell. Significant remodeling was noted in all cases; the shorter time intervals provided a better appreciation of the increase, decrease, or movement of individual focal contact sites. Remodeling did not consistently occur in any preferred direction in the cell; regions which expressed preferred directional changes were always associated with exploratory directional movement of cellular processes and/or cell migration. Area calculations indicated that 36, 43, and 54% of the total available focal contact site area was involved in remodeling during intervals of 5, 10, and 30 min, respectively, in the image series shown in Fig. 9. However, these are only estimates because entire small focal contact sites disappear and new ones appear within minutes as part of the continuous remodeling process; numerous examples of this can be seen in Fig. 9.

Quantitative information relevant to cell-substratum adhesion

After a TSCM image was digitized and processed, the radiance threshold was set over a narrow range (gray to black) to eliminate all but the regions of focal contact which were then assigned an identity in computer memory (Fig. 10). Two measurements, readily accessible in the digitized images, were made to nominally define cell adhesion; the area of each focal adhesion site, and the average radiance level of the pixels therein:

$$\text{Adhesion} = A(R)^{-1} \qquad [1]$$

where A = area of focal contact (square pixels), and R = average radiance levels of the pixels within any defined focal adhesion area. $(R)^{-1}$, the inverse radiance, represents the darkness of each pixel. Thus for a field circumscribing one cell, A is the area of all focal contact sites in the cell and $(R)^{-1}$ is the average darkness of those sites. Since all other image information from the cell was excluded (by a combination of the optical sectioning properties of the TSCM and by gray level thresholding of the digitized image), the image processing software rapidly calculated A, R, and adhesion value for any defined field. A wide range of images ranging from single focal adhesions to a field of several cells were available for analysis. Field size was varied primarily by the use of objective lenses of different magnifications with additional adjustment using the TSCM iris diaphragm. With a ×40 objective, a field of several cells was ob-

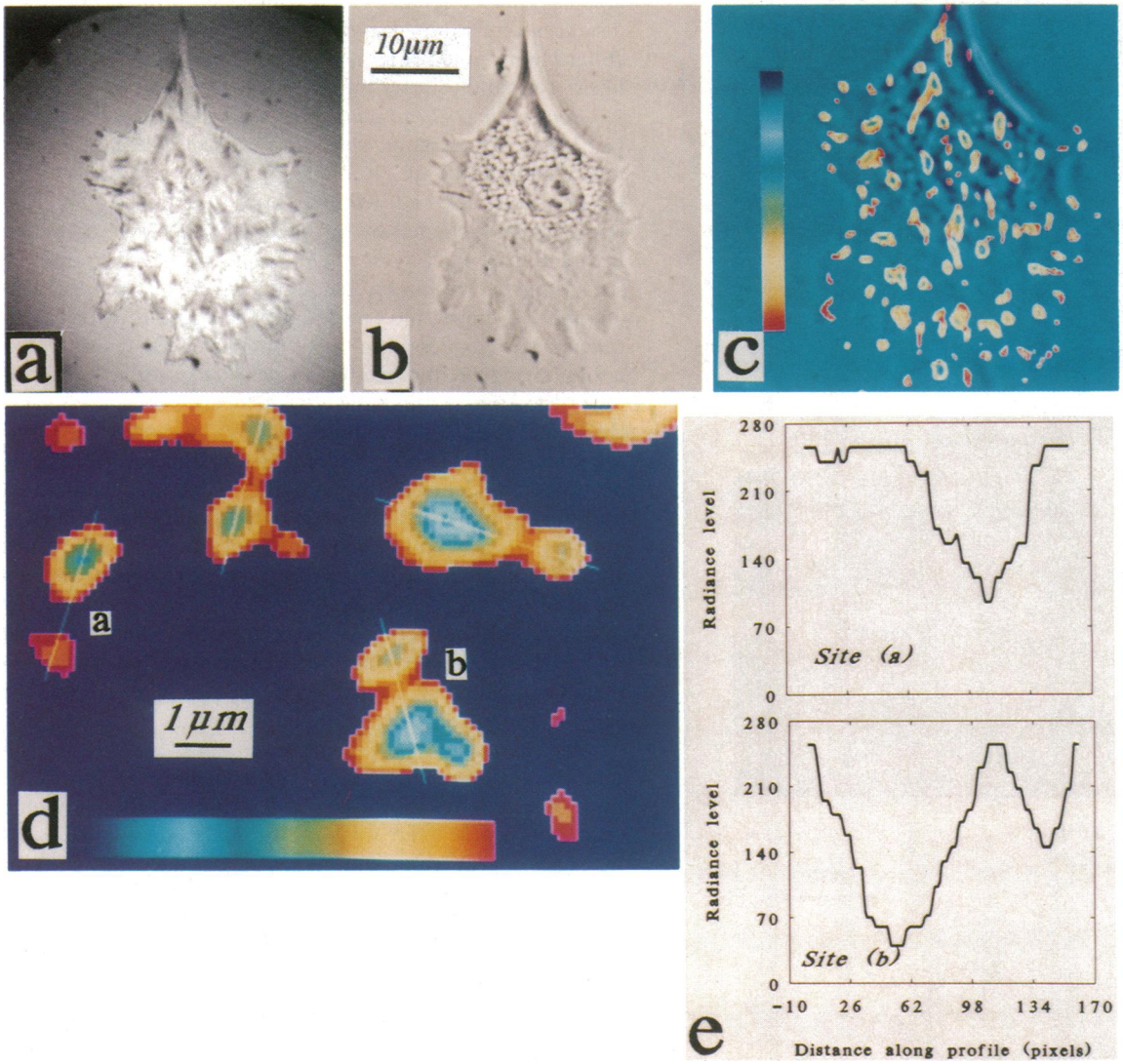

Figure 6. TSCM (*a*), phase contrast (*b*), and digitally processed (*c*) images of a single endothelial cell to demonstrate the extraction of focal contact image information by digital image analysis. In (*c*), focal contact sites are superimposed onto the phase contrast image. (*a, b*) ×750; (*c*) ×850. (*d*) Enlargement of individual focal contact sites expressed in pseudocolor. The differences in color reveal small differences in radiance levels between the edges and center of each focal adhesion. Within each focal contact region the radiance threshold was reduced to a narrow range where light blue represents near zero radiance (black) and 255 represents dark grey, thereby amplifying the small but real differences of radiance intensity within each site. (*e*) Radiance profiles through two representative focal contact sites of Fig. 4 *d*.

served for analysis; at ×100 with the field diaphragm stopped down, the raw image was restricted to part of a single cell. Once the image was digitized, however, the measurement of detailed portions of the cell was essentially unlimited because enlargement to the single pixel level using a zoom facility was routinely available as part of the standard image analysis program (examples of this application are shown in Fig. 13, see below). Thus, adhesion measurements were performed on single focal contact sites, single cells, or groups of several cells.

Adhesion remains constant despite extensive focal contact remodeling in unperturbed cells

As noted above, the individual focal adhesion sites in unperturbed cells undergo extensive remodeling over intervals of minutes. However, as shown for a 25-min period in Fig. 11, this occurs without a significant change in overall cell adhesion as determined using equation [1]. The mean adhesion value calculated during this period from four similar experiments (96 data points) in unperturbed cells was 99.4%±2.1 (SD).

Perturbation results in loss of cell adhesion with predictable average changes of focal contact area and radiance levels

When a single cell or a confluent monolayer of endothelial cells was exposed to the cytoskeleton-destabilizing drug cytochalasin, or to the proteolytic enzyme trypsin, cells retracted from each other and rounded up. As shown in Fig. 12 the area of focal contact declined (Fig. 12 *a*), accompanied by increased average radiance level (decreased image darkness; Fig. 12 *b*) as contact between the abluminal cell surface and the substratum was reduced. The relative changes in cell adhesion calculated

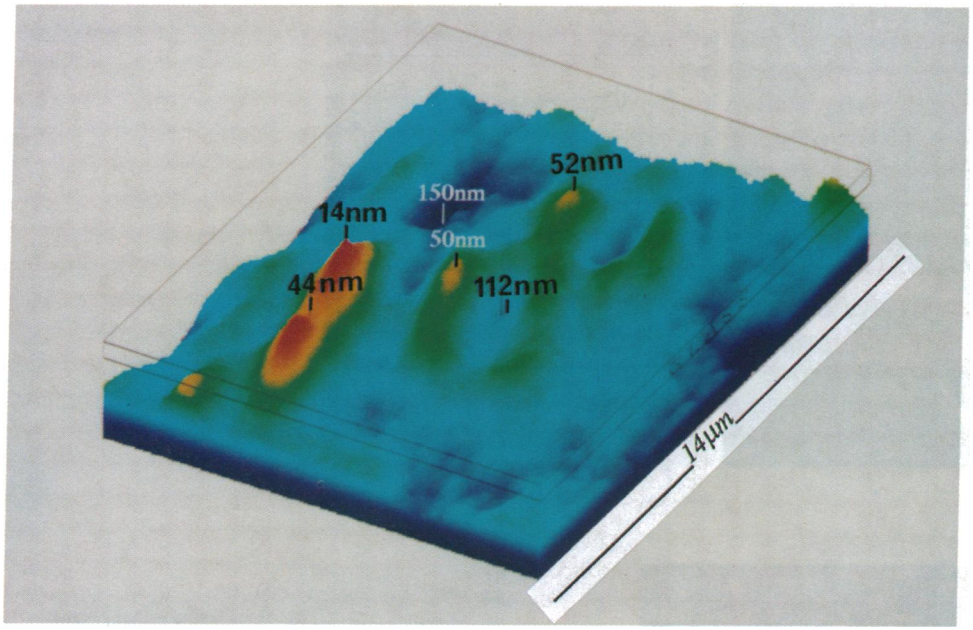

Figure 7. Topographical mapping of a 14 μm × 14 μm area of endothelial cell membrane in focal and close contact with the substratum. The cell is attached to the underside of the glass surface; membrane regions that come into focal and close contact with the glass appear as peaks. Separation distances between the cell membrane and the substratum were calculated from interference fringe calibrations; separation values are shown for a variety of sites in the 196-μm^2 area of profiled membrane. The scale of the z axis (peaks and valleys) is amplified in this figure (in comparison with the x and y axes) to better demonstrate the topographic relationship between cell and substratum.

by equation [1] are shown in Fig. 12 *c* (and for trypsin in Fig. 12 *c, inset*). These experiments demonstrated the utility of repeated measurements of the same cell in real time; the quantitative results are consistent with the loss of adhesion caused by the drug and enzyme manipulations.

The response to cytochalasin of a single focal adhesion site is shown in Fig. 13. During the 10-min period after addition of the drug, the site changed its shape (by remodeling) as well as its spatial relationship to the substratum. While there was an insignificant change of area (< 3%) the color distributions (Fig. 13 *a* and *b*) and profile graphs (Fig. 13, *c*) demonstrated increased separation between the cell and substratum.

Heterogeneous responses of focal adhesion within a cell subjected to perturbation

Despite an overall loss of adhesion in response to cytochalasin, individual focal contact sites responded with markedly varied kinetics. Some sites, particularly toward the central region of the cell, remained relatively unchanged for many minutes while others underwent disparate changes. Analyses of two sites are presented in Fig. 14. The first (Fig. 14 *a*) was relatively stable in size and radiance level before addition of the drug, after which contact with the substratum was progressively lost. In contrast, a second site (Fig. 14 *b*), which was rapidly remod-

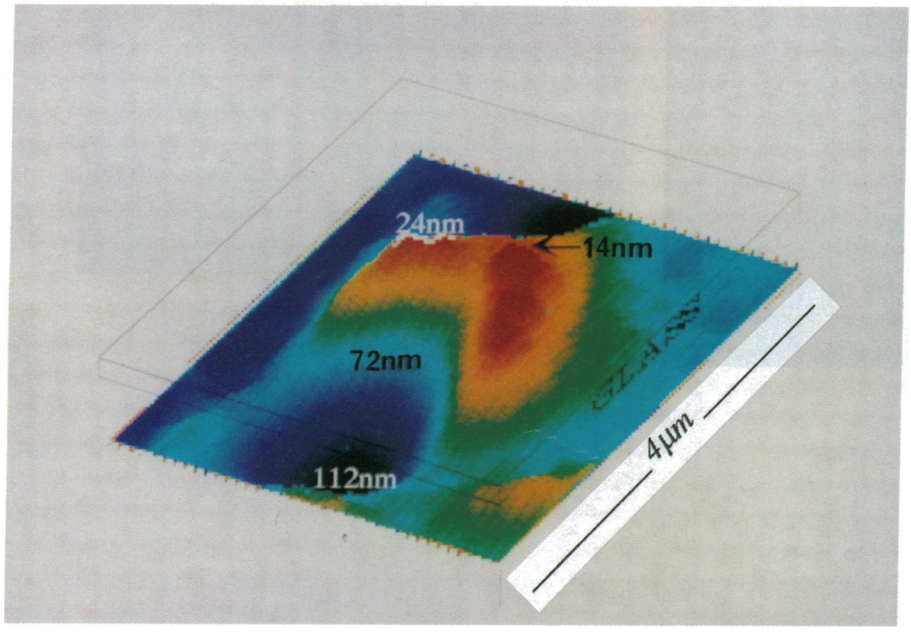

Figure 8. Detail of a single focal contact site which shows multiple point contacts where the topographic characteristics were regular. The estimated separation distances were estimated to be 14 nm at these points which may represent sites where cell membrane is distorted by actin stress fibers on the cytoplasmic side of the membrane.

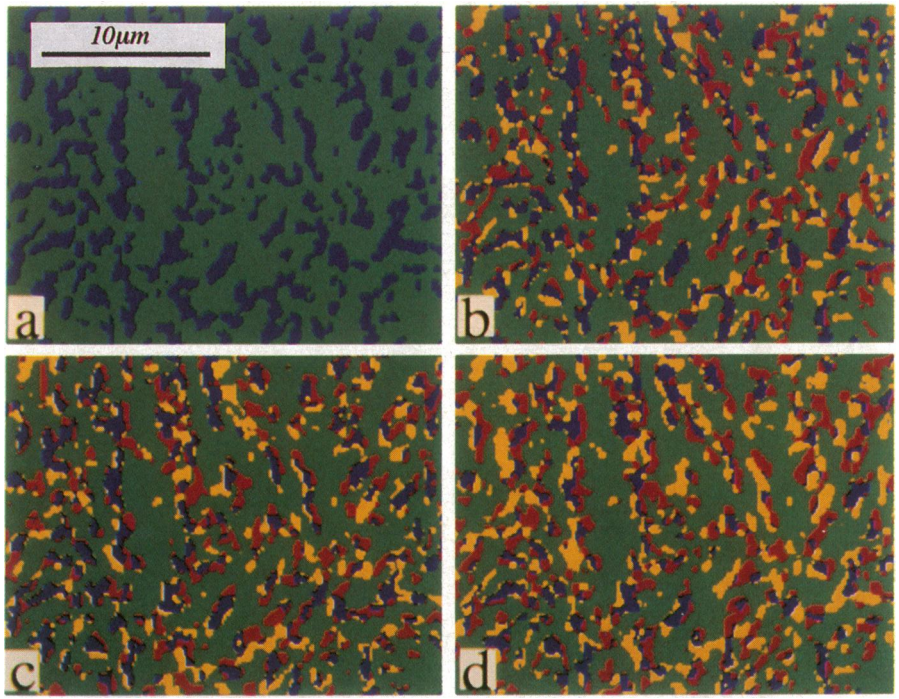
10μm
a
b
c
d

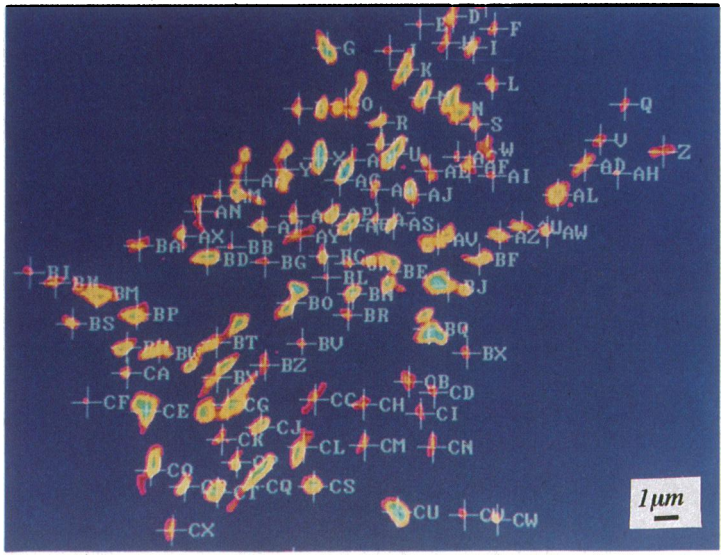
1μm

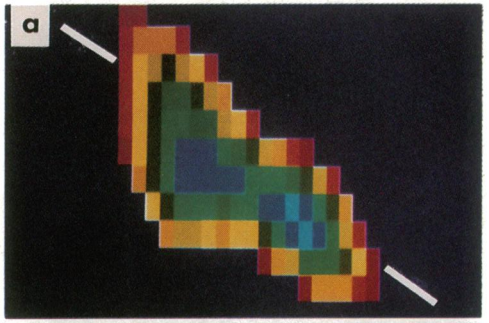
a
b
1μm

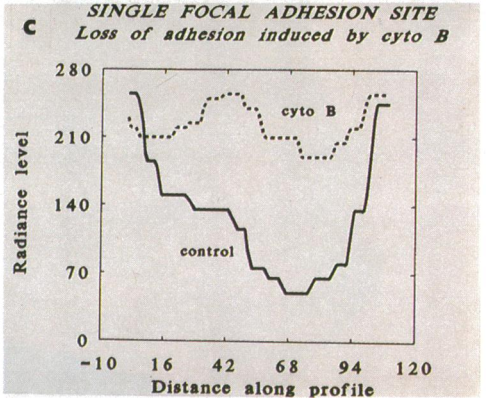
c
SINGLE FOCAL ADHESION SITE
Loss of adhesion induced by cyto B
Radiance level
280
210
140
70
0
cyto B
control
-10
16
42
68
94
120
Distance along profile

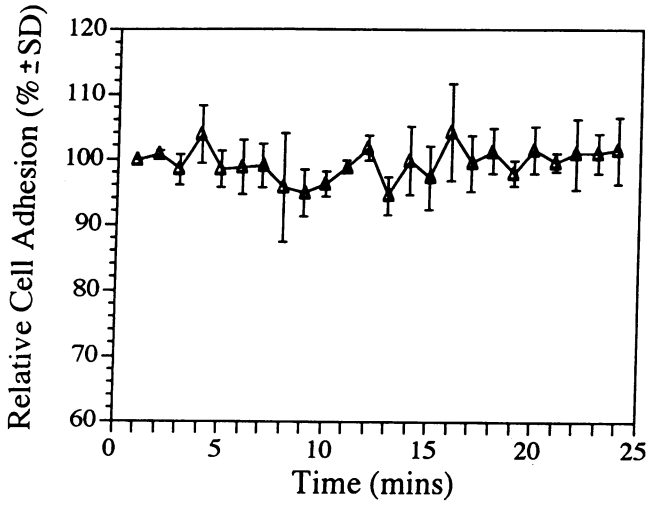

Figure 11. Cell adhesion as a function of time in a single endothelial cell. Cell adhesion was calculated using equation [1]. Each point is the mean±SD of four separate experiments; $n = 96$.

eling at the time that the drug was added, quickly stabilized its area and radiance levels such that adhesion was maintained constant for an extended period. These data demonstrate use of the technique to quantitate the kinetics of single focal contact regions in defined locations of the cell.

Discussion

Detailed studies of molecular interactions in living cells in real time have progressed significantly in recent years with the introduction of IRM (16), decoration of cell structures with fluorescent probes (28, 29), and both tandem scanning (30) and laser scanning (31) confocal microscopy. These methods provide information about cellular events in real time, and therefore allow the dynamics of cell behavior to be evaluated and, in some cases, quantitated. In addition, quantitative information about cell interactions with the substratum in fixed cells has recently been reported (32). In this paper we have used the optical capabilities of TSCM to observe the dynamics of focal contact sites in living endothelial cells and to determine cell adhesion in real time. The approach takes advantage of the development of hardware and software for image processing and analysis and focuses on focal contact sites, the principal structures responsible for adhesion of anchorage-dependent cells. The data demonstrate (*a*) that most focal adhesion sites continuously remodel, (*b*) that estimates of the detailed topography of the adhesion sites can be calculated from radiance measurements, (*c*) that it is feasible to measure the adhesion of a single cell, or part of a cell, over an extended period, (*d*) that

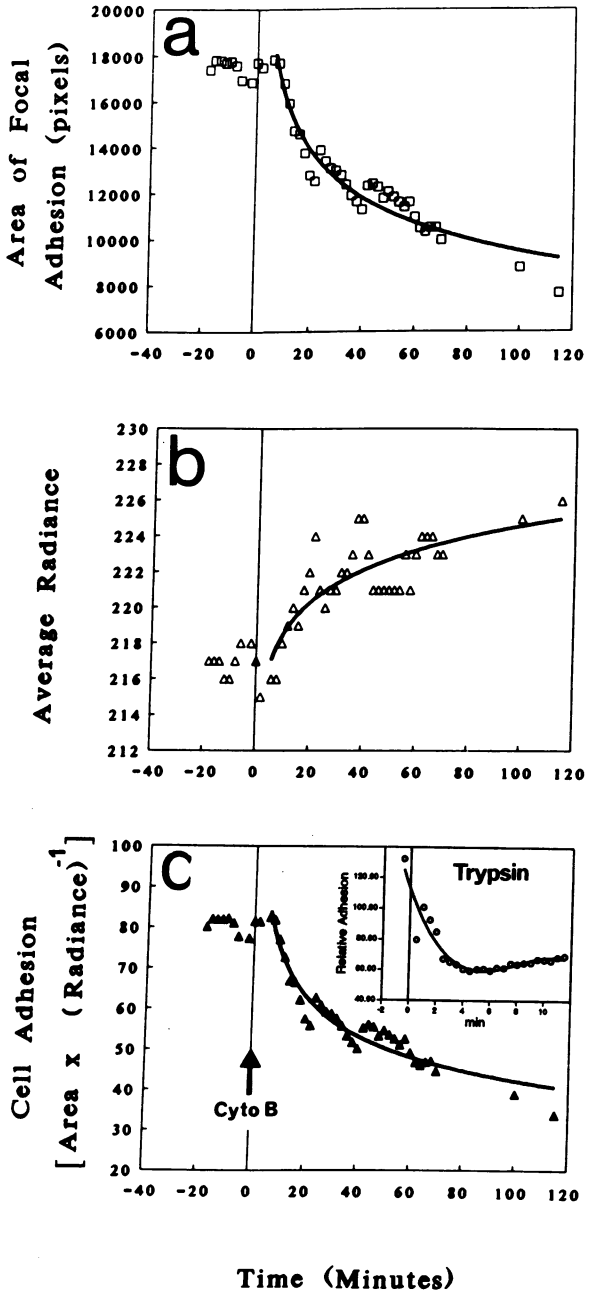

Figure 12. Repetitive measurements demonstrating loss of cell adhesion induced by cytochalasin (*a–c*) and trypsin (*inset c*). At t = 0, a single endothelial cell was exposed to cytochalasin B (10 μg/ml) or trypsin: EDTA. (*a*) Total area of focal contact sites in the cell. (*b*) Average pixel radiance level of focal contact sites. (*c*) Calculated cell adhesion.

Figure 9. (*top left*). Remodeling of focal contact sites (shown in blue in [*a*] at time 0) after 5, 10, and 30 min (*b, c,* and *d,* respectively) revealed by image subtraction in part of an unperturbed cell. In each of panels *b–d,* sites that remained unchanged are shown in blue while addition and loss of focal contact area are shown in red and yellow respectively. Confluent field of endothelial cells (one to two cells).

Figure 10. (*bottom left*). Processed TSCM image of focal contact sites in a single endothelial cell. The computer has stored digitized information obtained from each site, which has been assigned a letter identity. Quantitative information concerning individual sites or integration of all sites in the cell is readily accessible from the digitized area and radiance values.

Figure 13. Changes in a single focal contact site induced by cytochalasin. The site is shown immediately before (*a*) and 11 min after (*b*) addition of the drug. In addition to remodeling of the shape of the site, the pseudocolor distribution indicates decreased adhesion (increased radiance level) in the center. (*c*) Radiance profiles at locations indicated by the white lines in (*a*) and (*b*) confirm loss of adhesion; by interference calibration, the minimum separation distance is estimated to increase from 15 nm to 40 nm.

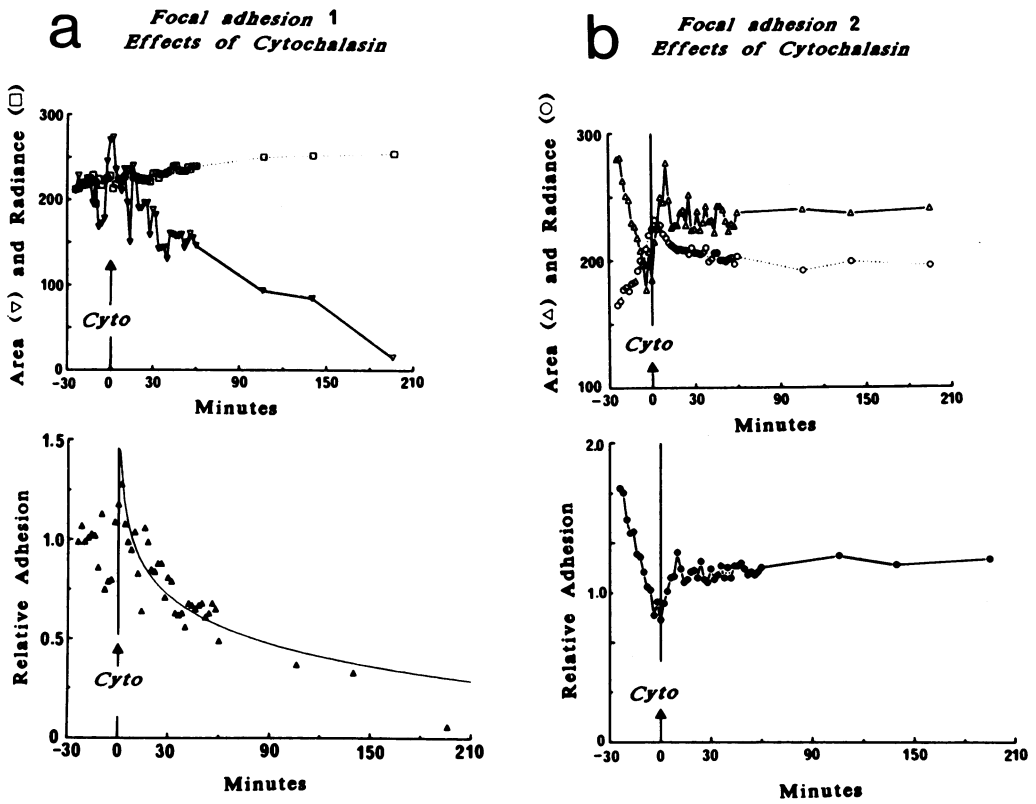

Figure 14. The responses of two individual focal contact sites to drug-induced perturbation. The sites were 3 μm apart in the cell. Each upper panel plots the area of focal contact (pixel area) and radiance level (arbitrary units) against time. Each lower panel plots the calculated adhesion of the site. Arrow indicates the time of exposure to cytochalasin. An area of 200 pixels represents ~ 4 μm^2 of membrane.

there is heterogeneity throughout the cell with respect to the kinetics of spontaneous focal adhesion assembly and disassembly as well as in response to experimental manipulation, and (*e*) that despite extensive changes in the distribution and kinetics of individual focal contact sites, the overall adhesion of endothelial cells varies by < 10% when the cells are left undisturbed.

Concerning the measurement of cell adhesion. Cell adhesion has usually been measured as the fraction of cells that attach to a defined substrate after plating. While this approach has provided much useful information concerning the relative effectiveness of different adhesion molecules, it fails to address the factors influencing steady-state adhesion in cultured cells. Attempts have been made to determine the resistance of cells to removal from culture surfaces by measuring the flow (14) or centrifugal forces (19) required for detachment. In general, however, these approaches do not provide continuous information about cell adhesion, and cell counts represent an average response of many cells. In the approach reported here, dynamic and quantitative information was obtained about the membrane/substratum sites regulating cell adhesion.

The TSCM acts as a confocal interference reflectance microscope in which high contrast IRM images are generated by thin layer optical properties at the cell–glass interface. The image observed arises from light that is differentially reflected at the interface between substances of different refractive indices. When observed by oil-immersion objectives with epi-illumination, the field appears uniformly bright when no cells are present because of strong reflection at the glass–liquid interface. When the cell surface is in very close contact with the glass, however, such as occurs at a focal adhesion, the high refractive index of the membrane decreases the reflection, less light returns through the microscope, and the image appears dark (24, 33). When there is separation between the cell and the substratum, light is reflected at both the glass–liquid interface and the liquid–cell interface and interference occurs to produce alternate bright and dark zones at separation distance intervals of $\lambda/4$ (163 nm). In the confocal microscope the optical plane was set in the underlying glass substratum such that it glanced the ventral cell surface and penetrated less than one wavelength into the cell. Thus multiple interference patterns resulting from wide separation of cell and substratum were reduced or eliminated, and additional reflective interfaces within the cell (such as nuclear–cytoplasmic and apical membrane–cytoplasmic interfaces) were avoided. The resulting image therefore was generated primarily by the abluminal membrane interactions with the glass substratum up to a separation distance of less than one half wavelength (325 nm; first order fringe minimum), and occasionally slightly higher (see calibration method in Methods).

Within separation distances of 0 to 163 nm, the radiance intensity increased as a function of the distance between cell and substratum, the interference being zero order in such areas when observed with objectives of numerical aperture > 1.0 (24). Consequently, by considering the area of focal contact in a cell and taking account of the radiance values within the focal contact sites, both qualitative and quantitative information about cell adhesion was obtained.

There is good evidence that the focal contact sites are specifically responsible for the adhesion of anchorage-dependent cells. Using IRM imaging of fibroblasts, Lotz et al. (19) have correlated the area of focal adhesions with the cell-substratum strength measured by a centrifugation technique. They noted a close correlation between the area of focal contact and the strength of adhesion on two dissimilar substrates, fibronectin and tenascin. Their data also extended the estimates, made by

Bell (34) and Lotz et al. (19), of critical forces required to detach cells ($0.4–1.0 \times 10^{-5}$ dyn/bond) in that the force required to remove 50% of a population of glial cells ($> 36 \times 10^{-5}$ dyn) was consistent with the sum of the fibronectin receptor clusters in focal contacts in each cell. Thus the area of focal contacts appears to provide a valid estimate of cell adhesion. We suggest that, in addition to area, differences in the average radiance levels of focal contact sites reflect small differences in adhesion avidity; the average radiance of all focal contacts in the cell changed in a predictable direction when adhesion was experimentally impaired. Consequently these differences, which arise because of altered focal contact profile with respect to the substratum, were included in the calculation of cell adhesion (equation [1]). The radiance profiles of individual adhesion sites consistently showed slightly greater contact at the center, raising the possibility of ordered arrays of different adhesion proteins arranged in the contact area or of lower affinity of binding between integrins and extracellular matrix in the periphery. Occasional profiles of point contact that were particularly visible in three-dimensional topographical maps were suggestive of the termination of actin bundles on the cytoplasmic side of the membrane presumably drawn there by the interaction between actin, linker proteins, and transmembrane integrins. Detailed monitoring of such sites in the presence of specific antibodies directed against integrin/adhesion protein may in the future provide insights into these complex interactions.

The technique for calibrating separation distances between cell and substratum is based upon straightforward interference optics. While the principles are sound, there will be small differences between the radiance curves in cells in different fields and different experiments. This is determined by the setting of the optical plane which, although every effort is made to standardize its position, will vary slightly within and between fields. However, the approach addresses several key questions. First, it shows unequivocally that the dark regions in the cell are indeed adhesion sites because separation distances were always < 50 nm. Second, it allows monitoring of adhesion topology. That is useful even if the separation distances may be slightly over or underestimated by the calibration fit; the relative numbers provide real time information. By setting the optical section primarily outside of the cell, multiple order interference fringes were avoided as were images of major cellular oganelles whose contribution to the refraction/reflection images would become a problem. In short, the calibration approach strongly supports our interpretation of the nature of the discreet regions of low radiance as focal contact sites.

Concerning remodeling of focal contacts. Spontaneous remodeling that occurred in all of the adhesion sites of unperturbed cells observed over a 30-min interval involved changes in $> 50\%$ of the total adhesion area of the cell. At shorter intervals, spatial differences in remodeling rates were more apparent. There was, however, no distinctive location of more active or less active sites within the cell, and adjacent focal adhesions often remodeled at greatly different rates (e.g., see Fig. 9).

The mechanism of remodeling is unclear. Filamentous actin fibers terminate at focal contact sites and are linked to specific transmembrane integrin proteins via linker proteins (1). The best characterized example of linkage is the binding of α-actinin to F-actin at one end of the molecule and to the integrin β_1 subunit at the other end (26). Other potential linkers include primarily vinculin, talin, and paxillin, all of which are localized to focal contact sites (1, 27) although they bind integrins with much lower affinities than does α-actinin (26). Disassembly and reassembly of some of these molecular associations are likely to be involved in the remodeling mechanism. During remodeling many sites gain and lose equal areas producing an appearance of site "migration." Given the dynamic equilibrium between soluble cytoplasmic pools and membrane-bound fractions of α-actinin, actin, and vinculin (4), it is likely that turnover of the elements on the cytoplasmic side of the membrane regulate extracellular changes in binding affinity to adhesion proteins. Binding affinities between microfilaments and linker proteins, or between linker proteins and intracellular domains of integrins, may be modified. When the contact sites appear to move, the intracellular changes must also induce disassociation of extracellular binding to adhesion molecules on the glass; otherwise the contact sites would simply grow as the membrane–glass interface failed to separate (a feasible mechanism when contact sites enlarge). Evidence supporting intracellular alteration of integrin adhesion to extracellular proteins has recently been demonstrated by O'Toole et al. (35). They showed altered binding affinity between αIIbβ3 integrin and fibrinogen after truncation of the cytoplasmic domain of the αIIb subunit. Transmembrane signaling through focal adhesions can also proceed from outside to inside. Qwarnstrom et al. (36) have shown that IL-1/IL-1 receptor interactions localized to sites of focal contact in fibroblasts produce loss of cell-substratum contact in part by mediating phosphorylation of talin via activation of a protein serine/threonine kinase. Phosphotyrosine proteins and tyrosine kinases are also concentrated at sites of focal contact (37, 38). During spontaneous remodeling of focal contact sites, it is unclear if protein conformational changes associated with phosphorylation events at the cytoplasmic side of the membrane can signal the dissociation/reassociation of integrins with extracellular adhesion proteins.

Digital image analysis of focal contact sites provides information about the adhesion of living cells in real time. It facilitates measurements of the effects of cellular manipulation upon cell adhesion at the sites structurally adapted to cell–substratum interactions. It is of particular interest in relation to our studies of the effects of flow on endothelial cells, the signal transduction mechanisms associated with such responses, and the role that cell tension plays in their regulation (22, 39, 40). When confocal techniques are combined with fluorescence microscopy of cytoskeletal components, particularly actin stress fibers, and with specific probes for the proteins of the adhesion complex, the mechanisms controlling the dynamics of focal adhesion should become clearer. In light of the large amount of emerging information concerning adhesion proteins, integrins, and proteins linking integrins to the cytoskeleton, it should be possible to use image analysis to interpret the interactions between molecules participating in adhesion in the living cell; in effect using the imaging of a biological structure in real time to analyze molecular function.

Acknowledgments

We thank Ken Barbee and Ratnesh Lal for atomic force microscopy measurements, Andrea Banega and Susan McKibben for technical assistance, and René Payne for preparation of the manuscript. We gratefully acknowledge discussions with Dr. George Truskey of Duke University and with Drs. Jonathan Art, Randal Dull, Godfrey Getz, Stephen Meredith, and Neil Smalheiser of the University of Chicago.

Supported by American Heart Association Grant in Aid 91-1557 (P. F. Davies), National Institutes of Health grants HL-36028 (P. F. Davies), HL-36049 (P. F. Davies), and CA27307 (M. L. Griem), and by the Work-Study program of the University of Chicago (A. Robotewskyj).

References

1. Burridge, K., K. Fath, T. Kelly, G. Nuckolls, and C. Turner. 1988. Focal adhesions. *Ann. Rev. Cell Biol.* 4:487–525.

2. Ingber, D. 1991. Integrins as mechanochemical transducers. *Curr. Opin. Cell Biol.* 3:841–848.

3. Heath, J. P., and G. A. Dunn. 1978. Cell to substratum contacts of chick fibroblasts and their relation to the microfilament system. A correlated interference reflexion and high voltage electron microscope study. *J. Cell Sci.* 29:197–212.

4. Geiger, B., Z. Avnur, T. E. Kreis, and J. Schlessinger. 1984. The dynamics of cytoskeletal organization in areas of cell contact. *Cell Muscle Motil.* 5:195–234.

5. Buck, C., and A. Horwitz. 1987. Integrin, a transmembrane glycoprotein complex mediating cell-substratum adhesion. *J. Cell Sci. Suppl.* 8:231–250.

6. Paddock, S. W. 1989. Tandem scanning reflected light microscopy of cell-substratum adhesions and stress fibres in Swiss 3T3 cells. *J. Cell Sci.* 93:142–146.

7. Stehbens, W. E. 1966. The basal attachment of endothelial cells. *J. Ultrastruct. Res.* 15:388–400.

8. Abercrombie, M., J. E. Heaysman, and S. M. Pegrum. 1971. The locomotion of fibroblasts in culture. IV. Electron microscopy of the leading lamella. *Exp. Cell Res.* 67:359–367.

9. Ts'ao, C.-H., and S. Glagov. 1970. Basal endothelial attachment. Tenacity at cytoplasmic dense zones in the rabbit aorta. *Lab. Invest.* 23:510–516.

10. Folkman, J., and A. Moscona. 1978. Role of cell shape in growth control. *Nature (Lond.).* 273:345–350.

11. Ingber, D., and J. Folkman. 1989. Mechanochemical switching between growth and differentiation during fibroblast growth factor-stimulated angiogenesis in vitro: role of extracellular matrix. *J. Cell Biol.* 109:317–325.

12. Hay, E. D., and S. Meier. 1976. Stimulation of corneal differentiation by interaction between cell surface and extracellular matrix. II. Further studies on the nature and site of transfilter induction. *Dev. Biol.* 52:141–157.

13. Gospodarowicz, D., G. Greenburg, and C. R. Birdwell. 1978. Determination of cellular shape by the extracellular matrix and its correlation with the control of cellular growth. *Cancer Res.* 38:4155–4171.

14. Pratt, K. J., B. E. Jarrell, S. K. Williams, R. A. Carabisi, M. A. Rupnick, and F. A. Hubbard. 1988. Kinetics of endothelial cell-surface attachment forces. *J. Vasc. Surg.* 7:591–599.

15. Nuckolls, G. H., C. E. Turner, and K. Burridge. 1990. Functional studies of the domains of talin. *J. Cell Biol.* 110:1635–1644.

16. Izzard, C. S., and L. R. Lochner. 1980. Formation of cell to substrate contacts during fibroblast motility: an interference-reflection study. *J. Cell Sci.* 42:81–116.

17. Murphy-Ullrich, J. E., and M. Hook. 1989. Thrombospondin modulates focal adhesions in endothelial cells. *J. Cell Biol.* 109:1309–1319.

18. Wechezak, A. R., T. N. Wight, R. F. Viggers, and L. R. Sauvage. 1989. Endothelial adherence under shear stress is dependent upon microfilament reorganisation. *J. Cell. Physiol.* 139:136–146.

19. Lotz, M. M., C. A. Burdsal, H. P. Erickson, and D. R. McClay. 1989. Cell adhesion to fibronectin and tenascin: quantitative measurements of initial binding and subsequent strengthening response. *J. Cell Biol.* 109:1795–1805.

20. Schwartz, S. M. 1980. Selection and characterization of bovine aortic endothelial cells. *In Vitro (Rockville).* 14:966–978.

21. Thornton, S. C., S. N. Mueller, and E. M. Levine. 1983. Human endothelial cells: use of heparin in cloning and long term serial cultivation. *Science (Wash. DC).* 22:623–625.

22. Olesen, S. P., D. E. Clapham, and P. F. Davies. 1988. Hemodynamic shear stress activates K^+ current in vascular endothelial cells. *Nature (Lond.).* 331:168–170.

23. Davies, P. F., H. G. Rennke, and R. S. Cotran. 1981. Influence of molecular charge upon the endocytosis and intracellular fate of peroxidase activity in cultured arterial endothelium. *J. Cell Sci.* 49:69–83.

24. Verschueren, H. 1985. Interference reflection microscopy in cell biology: methodology and applications. *J. Cell Sci.* 75:279–301.

25. Semich, R., and H. Robenek. 1990. Organization of the cytoskeleton and focal contacts of bovine aortic endothelial cells cultured on types I and III collagen. *J. Histochem. Cytochem.* 38:59–67.

26. Otey, C. A., F. M. Pavalko, and K. Burridge. 1990. An interaction between α actinin and the β_1 integrin subunit in vitro. *J. Cell Biol.* 111:721–729.

27. Turner, C. E., J. R. Glenney, and K. Burridge. 1990. Paxillin: a new vinculin-binding protein present in focal adhesions. *J. Cell Biol.* 111:1059–1068.

28. Sammak, P. J., and G. G. Borisy. 1988. Direct observation of microtubule dynamics in living cells. *Nature (Lond.).* 332:724–726.

29. Mittal, B., J. M. Sanger, and J. W. Sanger. 1987. Visualization of myosin in living cells. *J. Cell Biol.* 105:1753–1760.

30. Boyde, A., C. E. Dillon, and S. J. Jones. 1990. Measurements of osteoclastic resorption pits with a tandem scanning microscope. *J. Microsc. (Oxf.).* 158:261–265.

31. Shuman, H., J. M. Murray, and C. DiLullo. 1990. Confocal microscopy: an overview. *Biotechniques.* 7:154–163.

32. Truskey, G. A., J. S. Burmeister, E. Grapa, and W. M. Reichert. 1992. Total internal reflectance microscopy (TIRFM). II. Topographical mapping of relative cell/substratum separation distances. *J. Cell Sci.* 103:491–499.

33. Bereiter-Hahn, J., C. H. Fox, and B. Thorell. 1979. Quantitative reflection contrast microscopy of living cells. *J. Cell Biol.* 82:767–779.

34. Bell, G. I. 1978. Models for the specific adhesions of cell to cell. *Science (Wash. DC).* 200:618–627.

35. O'Toole, T. E., D. Mendelman, J. Forsythe, S. J. Shattil, E. F. Plow, and M. Ginsberg. 1992. Modulation of the affinity of integrin αIIbβ3 (gpIIb-IIIa) by the cytoplasmic domain αIIb. *Science (Wash. DC).* 254:845–847.

36. Qwarnstrom, E. E., S. A. MacFarlane, R. C. Page, and S. K. D. Dower. 1991. Interleukin Ib induces rapid phosphorylation and redistribution of talin: a possible mechanism of fibroblast focal adhesion. *Proc. Natl. Acad. Sci. USA.* 88:1232–1236.

37. Maher, P. A., E. B. Pasquale, J. Y. Juang, and S. J. Singer. 1985. Phosphotyrosine-containing proteins are concentrated in focal adhesions and intercellular junctions in normal cells. *Proc. Natl. Acad. Sci. USA.* 82:6576–6580.

38. Hyatt, J. L., T. Klanck, and S. Jaken. 1990. Protein kinase C is localized in focal contacts of normal but not transformed fibroblasts. *Mol. Carcinog.* 3:45–53.

39. Davies, P. F., and S. Tripathi. 1993. Stress mechanisms in cultured cells: an endothelial paradigm. *Circ. Res.* 72:239–245.

40. Robotewskyj, A., R. O. Dull, M. L. Griem, and P. F. Davies. 1991. Dynamics of focal adhesion site remodelling in living endothelial cells in response to shear stress forces using confocal image analysis *FASEB (Fed. Am. Soc. Exp. Biol.) J.*, 5:A527 (Abstr.)